# Construction and validation of transcription-factor-based prognostic signature for TACE non-response and characterization of tumor microenvironment infiltration in hepatocellular carcinoma

JIAPENG SHI[1*], XINTONG WEI[2*], FANGMEI JIANG[3], JIANJUN ZHU[3], JIANDONG SHEN[4] and YANJUN SUN[3]

[1]Department of Interventional Medicine, Nantong Traditional Chinese Medicine Hospital, Nantong, Jiangsu 226001, P.R. China;

[2]Department of Medical Imaging, Nantong Traditional Chinese Medicine Hospital, Nantong, Jiangsu 226001, P.R. China;

[3]Department of Oncology, Yancheng Tinghu District People's Hospital, Yancheng, Jiangsu 224000, P.R. China;

[4]Department of Invasive Technology, Affiliated Nantong Hospital 3 of Nantong University, Nantong, Jiangsu 226001, P.R. China

**Abstract.** Hepatocellular carcinoma (HCC) is one of the most common malignant tumors worldwide. Despite continuous development of treatment methods, overall survival rate of liver cancer is low. Transcatheter arterial chemoembolization (TACE) is a first-choice treatment for advanced liver cancer. Although it is generally effective, a number of patients do not benefit from it. Therefore, the present study was conducted to assess the response of patients following TACE. RNA-sequencing data and corresponding clinical information were extracted from The Cancer Genome Atlas (TCGA) and Gene Expression Omnibus databases. Models were constructed using weighted gene co-expression network analysis and least absolute shrinkage and selection operator-Cox regression analysis based on TCGA-LIHC and GSE104580 cohorts. The receiver operating characteristic curve was used for evaluation. Immunoassay, half-maximal inhibitory concentration analysis of risk groups, genomic enrichment analysis and nomogram construction were also performed. The predictive models were validated at the single-cell level using single-cell databases. Finally, the present study examined the expression of TACE refractoriness-related TFs (TRTs) in TACE-resistant and non-resistant cell lines *in vitro*. A risk categorization approach was created based on screening of four TRTs. The patients were split into high- and low-risk groups. There were significant variations in immune cell infiltration, medication sensitivity and overall survival (OS) between patients in the high-risk and low-risk groups. Multivariate Cox regression analysis showed that the risk score was an independent prognostic factor for OS. In the single-cell gene set, risk score was a good indicator of tumor microenvironment (TME). Reverse transcription-quantitative PCR revealed that three high-risk TRTs were upregulated in TACE-resistant cells. Prognosis and TME status of liver cancer patients following TACE could be assessed using a predictive model based on transcription factor correlation. This predictive model provided a reliable and simplified method to guide the clinical treatment of HCC.

*Correspondence to:* Professor Yanjun Sun, Department of Oncology, Yancheng Tinghu District People's Hospital, 66 Zhongting Middle Road, Tinghu, Yancheng, Jiangsu 224000, P.R. China
E-mail: 8994518@qq.com

Professor Jiandong Shen, Department of Invasive Technology, Affiliated Nantong Hospital 3 of Nantong University, 60 Middle Qingnian Road, Nantong, Jiangsu 226001, P.R. China
E-mail: shenjiandong_78722@163.com

*Contributed equally

## Introduction

Hepatocellular carcinoma (HCC) ranks sixth and third in terms of global cancer morbidity and mortality, respectively (1). Liver cancer has become a major public health

problem. Hepatitis B is one of the most important causes of liver cancer (2). The main pathological types of liver cancer include HCC and cholangiocarcinoma and HCC accounts for nearly 80% of cases. Early symptoms of liver cancer are not obvious; therefore, most patients are diagnosed at a middle or advanced stage. At present, surgical resection is the main treatment method for liver cancer worldwide and other methods such as transcatheter arterial chemoembolization (TACE), radiotherapy and immunotherapy are auxiliary (3). However, the benefits of various treatments are limited and overall survival (OS) remains low. Therefore, it is necessary to explore the causes of liver cancer recurrence after treatment and intervene to improve treatment efficacy.

TACE is a first-line treatment for unresectable HCC. The principle of TACE involves selectively or superselectively inserting a catheter into the tumor-feeding artery, followed by administration of embolic and chemotherapeutic agents. This induces ischemic necrosis of the tumor, thereby inhibiting its progression and improving quality of life.

Depending on the operation time and method, TACE can be divided into assistant, conventional and drug-eluting TACE (4). However, there remains some controversy surrounding TACE. Due to the use of chemotherapeutic drugs, some patients experience a transient decrease in liver function following surgery (5). Furthermore, the abundant blood supply of liver cancer, production of new blood vessels following TACE, establishment of collateral circulation and other factors have made it difficult to achieve ideal therapeutic effects with simple TACE (6). There are also significant differences in the efficacy of TACE for different patients. To address this, the Japan Society of Hepatology introduced and subsequently revised the concept of TACE failure/refractoriness to improve evaluation of patient responses (7).

Investigation of the molecular mechanisms underlying TACE resistance is crucial for improving its therapeutic efficacy (8). In recent years, the combination of TACE with systemic therapies, particularly targeted therapies and immune checkpoint inhibitors (ICIs), has shown potential in prolonging progression-free survival and enhancing OS (9). For example, the combination of TACE with targeted drugs such as sorafenib and lenvatinib, as well as immunotherapies such as pembrolizumab, has demonstrated synergistic effects in several studies (10-12). However, despite the promising outcomes in some patients, the overall prognosis for HCC remains suboptimal, partly due to the development of resistance and recurrence following TACE (13). Consequently, further research into the mechanisms of TACE resistance and their interaction with combination therapy is essential for optimizing treatment protocols and improving patient outcomes.

Transcription factors (TFs) are proteins that regulate the transcription of genetic information from DNA to mRNA by binding to specific DNA sequences (14). TFs ensure that various genes are expressed inside the cell at the right time and in the right amount. There are >1,600 TFs in humans and most of them are involved in regulating a variety of important cellular functions, including division and death, as well as embryonic development (15). TFs are closely related to the occurrence and development of tumors. E-box binding zinc finger protein 2 can bind to the hepatitis B virus (HBV) core promoter, thereby inhibiting its activity and reducing the occurrence of HBV-induced liver cancer (16). Transcription termination factor (TTF)1 can affect proliferation of hepatoma cells by regulating the activity of ribosomes (17). Metastasis of liver cancer is also regulated by TFs, such as the transcription factor forkhead box P4, which can enhance its expression by directly binding to the promoter region of the *SLUG* gene and then transcribe a series of proteins downstream of *EMT* to promote liver cancer metastasis (18). TFs can regulate genes related to drug resistance, such as *MDR1* and *TWIST*. At present, research on the role of TFs in TACE resistance remains limited and further exploration is needed.

The present study combined TFs with TACE resistance and used weighted gene co-expression network analysis (WGCNA) to screen out *HUB* genes related to TACE nonresponse. Least absolute shrinkage and selection operator (LASSO)-Cox regression was used to build a prognosis-related predictive model and possible roles of TFs in the model of TACE resistance were analyzed in relation to immune microenvironment, drug sensitivity, single cells and cell experiments. It is expected that the present study will serve as a new resource for determining TACE effectiveness and the best course of treatment for liver cancer.

**Materials and methods**

*Datasets and preprocessing.* The present study included sequencing data (TPM format) from TCGA-LIHC (portal.gdc.cancer.gov/). Patients with incomplete follow-up information, 0 days of survival and repeated sequencing samples from the same patient were excluded. A total of 365 tumor samples were included for bioinformatics analysis and model construction. With same inclusion criteria, 231 HCC patients in the ICGC-LIHC (https://dcc.icgc.org/projects/LIRI-JP) cohort and 221 in the GSE14520 dataset were included for external validation. To identify genes associated with TACE resistance, the GSE104580 cohort (100 TACE responders and 100 non-responders) in the GEO database (https://www.ncbi.nlm.nih.gov/geo/) was obtained and further analysis was performed. When performing internal and external validation, the sva R package (v3.46.0) (19) was used for background correction and normalization to ensure comparability of validation (Fig. S1). A total of 1,639 TFs were extracted based on previous studies (20-22). GSE125449 is a single-cell sequencing set for LIHC and its processing pipeline is from the TISCH database. R software (version 4.0.5) (23) was used to conduct all of the analyses.

*Differentially expressed TF identification and enrichment analysis.* In GSE104580, differentially expressed genes (DEGs) between different response states were identified using the limma R package (version 3.52.0) (24) with $P<0.05$ and $|log2FC|>0.5$ as thresholds; adjusted $P<0.05$. The top 20 up-/downregulated differentially expressed TFs (DETFs) were plotted using the pheatmap R package (version 1.0.12) (25) after intersection with 1,639 TFs.

Gene Ontology (GO) was used to annotate the biological process, molecular function and cellular component of genes. Gene pathways were annotated using the Kyoto Encyclopedia of Genes and Genomes (KEGG). Significantly enriched pathways were indicated by P-values and q-values <0.05. The

clusterprofiler R package (v4.4.0) (26) was used for enrichment analysis of DETF-related functions and pathways (GO and KEGG), with P<0.05 as the threshold.

*TACE refractoriness-related TFs identification and enrichment analysis.* The present study took as input the ensemble of TFs in GSE10458 and removed genes with a standard deviation of 0 in each sample. To eliminate outlier genes and samples, R software package WGCNA goodSamplesGenes technique (version 1.68) (27) was used. WGCNA was then used to create a scale-free co-expression network. A soft threshold of 1-25 was used for topological calculations and the relation matrix was converted into an adjacency matrix using the best soft threshold. A topological overlap matrix (TOM) was created from the results and average link hierarchical clustering was performed. TOM classification of the associated modules was used and each module had ≥50 genes. The modules with a distance of <0.8 were combined and the correlation between the combined modules and TACE response was calculated. Finally, the DETFs and TFs in the co-expressed core module were overlapped and the identified TFs were used as TACE refractoriness-related TFs (TRTs). Enrichment analysis further explored the potential functions of DETFs and enriched pathways (GO and KEGG) using the clusterprofiler package, with P<0.05 as the threshold.

*Construction of a nomogram and prognostic model.* TCGA-LIHC cohort was used for modeling and the GSE14520 and ICGC-LIHC cohorts for external validation. In TCGA-LIHC, univariate Cox regression analysis was first used to filter out TFs with no prognostic significance in TRTs (P<0.05). To prevent overfitting effects, using LASSO regression, 10-fold cross-validation and 1,000 cycles with 1,000 random stimulations, a risk model was developed. The risk score formula was established by multivariate Cox regression analysis (stepwise) with integration coefficients and gene expression values. The patients were divided into high-risk and low-risk groups based on the median value of the risk score formula. Univariate and multivariate Cox regression analyses were used to assess the prognostic value of risk scores across the entire dataset and an external validation dataset. Time-dependent receiver operating characteristic (ROC) curves were used to compare the predictive accuracy of risk scores with traditional clinicopathological parameters. Prognostic nomograms were constructed using the replot R package (version 1.0.0) (28) and validated using calibration curves.

*Immune landscape analysis.* To assess the quantity of immune cells in various samples, several methods were used simultaneously, including TIMER (version 2.0) (29), CIBERSORT (version 1.06) (30), QUANTISEQ (version 1.0) (31), MCP-counter (version 1.2.0) (32), XCELL (version 1.1.0) (33) and EPIC (version 1.1) (34). In addition, the ESTIMATE algorithm (v1.0.13) (35) was used to calculate the immune score; the interstitial score to reflect the microenvironmental status (36). The tumor microenvironment (TME) is constructed by a variety of cell types. Thorsson *et al* (37) defined six immunoexpression signature subtypes based on the gene expression profile of all solid tumors in TCGA, including:

Wound Healing (Immune C1), IFN-γ Dominant (Immune C2), Inflammatory (Immune C3), Lymphocyte Depleted (Immune C4), Immunologically Quiet (Immune C5) and TGF-bβ Dominant (Immune C6). The present study classified patients based on immune expression signatures.

*Drug sensitivity analysis.* The present study obtained (38) half-maximal inhibitory concentration ($IC_{50}$) values of commonly used chemotherapeutic drugs for liver cancer from the Genomics of Cancer Drug Sensitivity (GDSC) database (https://www.cancerrxgene.org/) and used R software. The PRrophytic R package (v1.0.2) (39) was used for calculation. By using the Wilcoxon signed rank test, the differences in $IC_{50}$ between various risk categories were examined. Boxplots were used to depict the results.

*Cell lines and culture conditions.* Every cell line was bought from the National Certified Cell Center for Cultural Collections (Shanghai, China). Huh7 cells were cultured in Dulbecco's modified Eagle's medium (Gibco; Thermo Fisher Scientific, Inc.) supplemented with 1% penicillin-streptomycin and 10% fetal bovine serum. SNU-387 cells were cultured in RPMI medium (HyClone; Cytiva) supplemented with 10% fetal bovine serum and 1% penicillin-streptomycin. A cell incubator was used for cell culture, which was performed at 37°C with 5% $CO_2$ and 10% humidity. The cell lines used in the presence of mycoplasma were investigated in the present study.

*Protein staining.* Tumor tissue samples were fixed with 10% formalin at room temperature for 24 h. Subsequently, the samples were embedded in paraffin and sectioned at a thickness of 4 microns to allow for optimal staining and microscopic observation. Antigen retrieval was conducted at 95°C using citrate buffer (pH 6.0) to expose antigenic sites, followed by washing with phosphate-buffered saline (PBS) three times for 5 min each. Endogenous peroxidase activity was blocked using 3% hydrogen peroxide at room temperature for 10 min to prevent non-specific background staining. The sections were incubated with rabbit anti-XYZ antibody (cat. number: ab11174; Abcam), at a dilution of 1:200 at 4°C overnight, and detection was performed using DAB substrate and sections were counterstained with 0.1% hematoxylin solution at room temperature for 5 min. Images were captured using a light microscope at 40x magnification to document the staining results and assess the presence and localization of the target protein within the tissue samples.

*Cell viability and drug sensitivity.* Cells were seeded in 96-well plates at 5,000 cells/well and placed in a 37°C, 5% $CO_2$ incubator for 48 h. To simulate the TACE environment, another set of cells was placed in a 37°C, 5% $CO_2$, 1% $O_2$ incubator for 48 h. According to the concentration gradient, the experimental group was treated with lobaplatin (cat. no. H20050309; Hainan Changan International Pharmaceutical Co. Ltd.). The plates were taken out of the incubator after 48 h and put in a dark place so that 10 $\mu$l of CCK8 reagent (cat. no. A311-02; Vazyme Biotech Co., Ltd.) could be added to each well. The plates were returned to the incubator for 1-2 h. Optical density was determined using a microplate reader, (Multiskan FC; Thermo Fisher Scientific, Inc.).

*Reverse transcription-quantitative (RT-q) PCR*. For RNA extraction, ~5,000 cells per well were seeded in a 96-well plate. RNA isolation kit (cat. no. RC112-01; Vazyme Biotech Co., Ltd.) was used to extract total RNA and a cDNA synthesis kit (cat. no. R233-01; Vazyme Biotech Co., Ltd.) was used to create cDNA. All steps were performed according to the manufacturer's protocols. Using SteponePlus (Applied Biosystems; Thermo Fisher Scientific, Inc.), RT-qPCR was performed using 10 $\mu$M primers and SYBR qPCR Master Mix (cat. no. Q511-02; Vazyme Biotech Co., Ltd.). PCR cycling conditions were as follows: Initial denaturation at 95˚C for 2 min, followed by 40 cycles of denaturation at 95˚C for 30 sec, annealing at 60˚C for 30 sec, and extension at 72˚C for 1 min. The relative expression levels were determined using the $\Delta\Delta$Cq method (40). Relative expression values were normalized to the control gene (GADPH). The primer pairs used in the present study are shown in Table I.

*Statistical analysis*. For the $IC_{50}$ results, statistical analysis of optical density values was performed using GraphPad Prism version 8.0 (Dotmatics). Data are presented as mean ± standard deviation derived from three independent experiments conducted in triplicate (n=3). For the RT-qPCR, the data were represented as mean ± SD from three independent experiments (n=3). The statistical significance of differences in gene expression levels between the two cell lines was evaluated using an unpaired Student's t-test. The statistical analyses were performed using GraphPad Prism version 8.0 (Dotmatics). P<0.05 was considered to indicate a statistically significant difference.

**Results**

*Identification of specific TRTs*. To explore potential TRTs in HCC, a differential gene expression study was conducted in the GSE104580 dataset on patients who had TACE responses and those who had none. Among 1,639 TFs, 158 DETFs were identified using the limma package, including 78 up- and 80 downregulated (P<0.05; |log2FC|>0.5). The heat map showed the top 20 upregulated (Fig. 1A) and downregulated (Fig. 1B) DEGs and DETFs. The clusterProfiler package was used to analyze the DETFs. Fig. 1C shows the top 20 KEGG signaling pathways that may be related to TACE responses, including 'transcriptional misregulation in cancer', 'circadian rhythm', 'herpes simplex virus 1 infection', 'hepatitis B', 'human T-cell leukemia virus 1 infection' and 'amphetamine addiction'. Fig. 1D-F shows GO terms that may be related to the TACE response. The cellular component part mainly included 'transcription factor complex', 'nuclear', 'transcription factor complex', 'RNA polymerase II transcription factor complex', 'protein-DNA complex' and 'nuclear chromatin'; the biological process part mainly included 'primary miRNA transcription by RNA polymerase II', 'tissue development', 'cell fate commitment', 'endocrine system development', 'DNA-templated transcription' and 'initiation'; and the molecular function part mainly included 'enhancer-sequence-specific DNA binding', 'enhancer binding' and 'RNA polymerase II distal enhancer sequence-specific DNA binding'.

With a good association with TACE response, WGCNA was used to build co-expression networks and modules

Table I. PCR primer sequences.

| Gene | Primer |
|---|---|
| *CENPA* | Forward: AAGAGCACACACCTCTTGATAA |
| | Reverse: CATGTAAGGTGAGGAGATAGGC |
| *KLF2* | Forward: CTTCGGTCTCTTCGACGAC |
| | Reverse: GTAGCTGCAGGTGTGAGTG |
| *CBX2* | Forward: GACTTAGATGCTAAGAGGGGTC |
| | Reverse: CTTCTTCCGGATGGGATCCTTC |
| *KCMF1* | Forward: GTGGATCACGAGGTTAGTTCAGGAC |
| | Reverse: CCGAGTAGCAGGAATTACAGGCATC |

containing the DETFs. All TFs in GSE10458 were used as input genes for WGCNA. After determining the optimal soft threshold of 5 (Fig. 2A), according to the dynamic tree-cutting technique, all of the TFs were clustered using a TOM-based dissimilarity metric, partitioning the tree into eight modules (Fig. 2B). The correlation of each module with TACE response was calculated (Fig. 2C). The blue module showed a strong positive correlation with TACE response (Fig. 2D). The GO and KEGG pathway enrichment results of the 212 TFs in the co-expressed blue module were similar to the previous enrichment results for DETFs. The KEGG pathways mainly included 'transcriptional misregulation in cancer', 'inflammatory bowel disease', 'Th1 and Th2 cell differentiation', 'Th17 cell differentiation' and 'hepatitis B' (Fig. 2E). The GO terms mainly included 'transcription initiation from RNA polymerase II promoter', 'cell fate commitment', 'intracellular receptor signaling pathway' and 'embryonic organ development' (Fig. 2F). The 158 DETFs in the aforementioned TACE response and nonresponse and the 212 TFs in the co-expressed blue module were overlapped and 65 TFs as TRTs were identified for subsequent analysis.

*Construction of a prognostic TRT signature*. To identify key TRTs associated with TACE response, univariate Cox regression analysis was used to identify TRTs significantly associated with prognosis in TCGA-LIHC cohort (Fig. 3A). The present study obtained 28 TRTs associated with prognosis (all P<0.05). Based on univariate Cox regression analysis, redundant TRTs were removed using LASSO regression analysis (enter method) for further screening (Fig. 3B). The best eigenvalue was 8. Multivariate Cox regression analysis (stepwise method) was performed on the eight TRTs following LASSO regression and four TRTs involved in modeling were identified, namely CENPA, KLF2, KCMF1 and CBX2 (Fig. 3C). A risk score was calculated for each patient based on the coefficients and expression levels of each TRT (Fig. 3C to assess prognosis. The heat map showed the expression of the four TRTs in the high- and low-risk groups, as well as the relationship between the high- and low-risk groups and the associated traits (Fig. 3D). ROC curves for 1-, 3- and 5-year survival prediction of patients showed that an area under the curve >0.7 indicating the ability to strongly predict prognosis (Fig. 3E). Kaplan-Meier analysis showed that patients with low risk scores had significantly longer survival times than patients
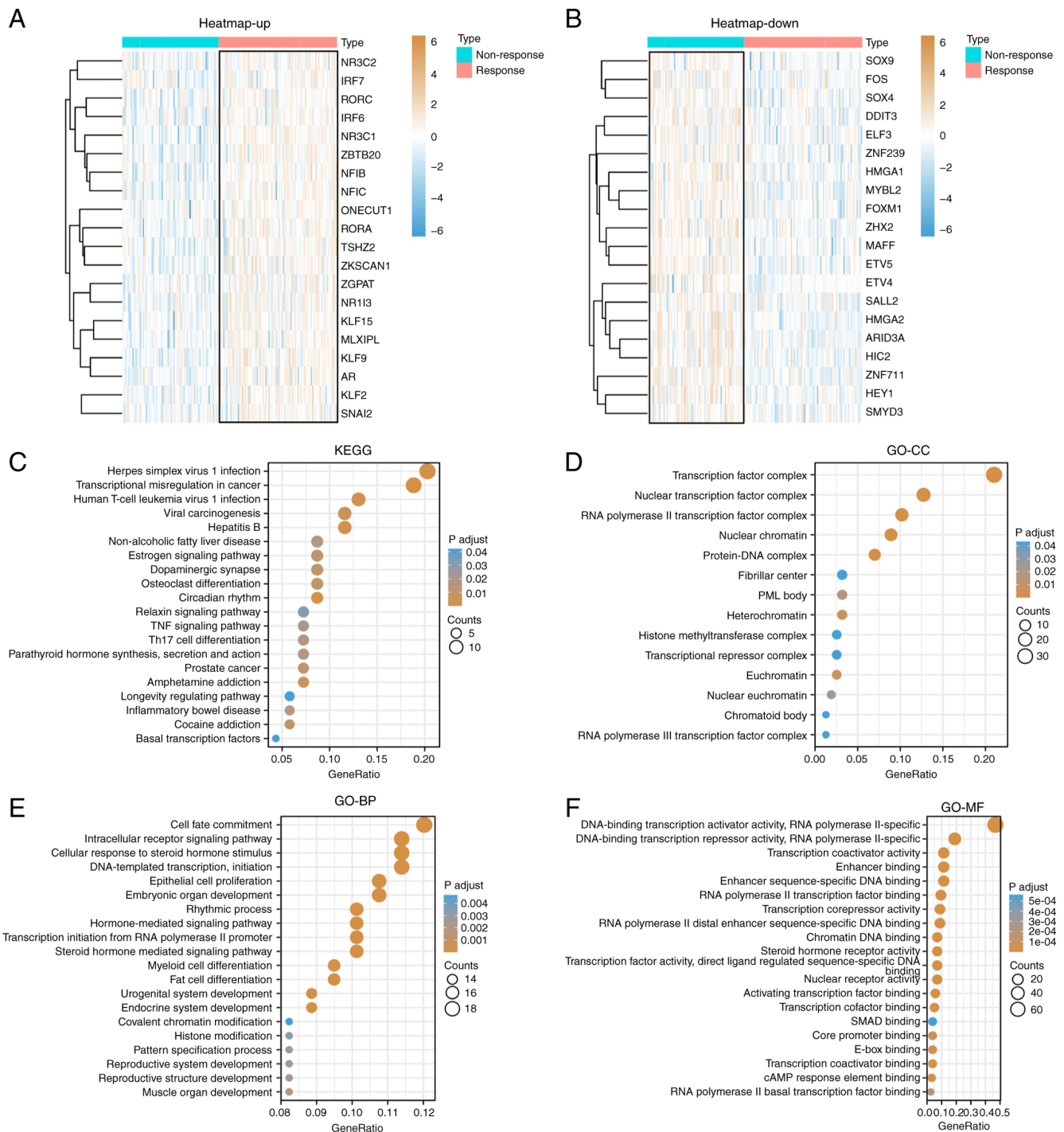
Figure 1. Landscape of TRTs in TCGA cohort and functional analysis. Heat map of the (A) upregulated and (B) downregulated TRTs between nonresponse and response patients. (C) KEGG and (D-F) GO analysis of TRTs. TRTs, TACE refractoriness-related transcription factors; TCGA, The Cancer Genome Atlas; KEGG, Kyoto Encyclopedia of Genes and Genomes; GO, Gene Ontology; CC, cellular component; BP, biological process; MF, molecular function.

with high risk scores (Fig. 3F). The risk distribution map also showed that survival time decreased significantly with increasing risk score (Fig. 3G and H). The prognostic value of the risk signatures were assessed according to risk score, age, sex, tumor stage and tumor grade. According to univariate Cox regression analysis, the risk score was significantly associated with OS [hazard ratio (HR)=1.544, 95% confidence interval (CI)=1.369-1.742] (Fig. 4A). Multivariate Cox regression analysis showed that risk score was an independent prognostic factor (HR=1.426, 95% CI=1.247-1.631) (Fig. 4B). Nomograms

and calibration plots were used to quantify the contribution of individual factors to clinical prognosis and validate the model (Fig. 4C and D). The prognostic model had good predictive ability in the three cohorts (TCGA, ICGC and GSE14520). The predicted line segments in the calibration curves in the different datasets were all close to the actual line segments.

*Validation of prognostic TRT signature in the external datasets.* The present study risk-scored patients in the external validation cohort ICGC-LIHC and the GSE14520 dataset using the
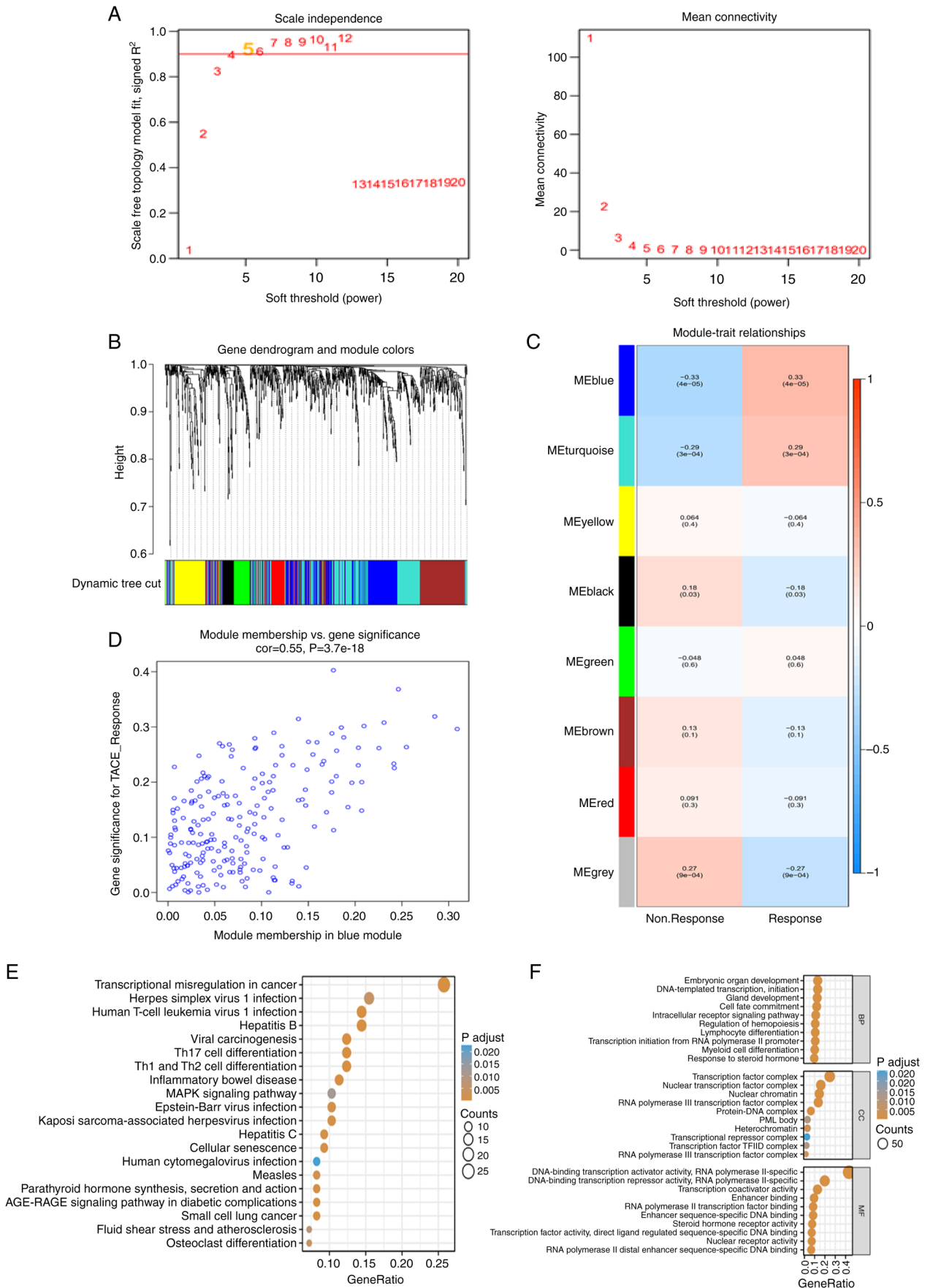
Figure 2. WGCNA was used to construct coexpression networks and modules of DETFs with strong correlation with TACE response. (A) Determining the optimal soft threshold for WGCNA. (B) Clustering all TFs using TOM-based dissimilarity measure. (C) Correlation of each module with TACE response. (D) Blue modules show a strong positive correlation with TACE response. (E) GO and (F) KEGG analysis of blue module genes. WGCNA, weighted gene co-expression network analysis; DETFs, differentially expressed transcription factors; TACE, transcatheter arterial chemoembolization; TFs, transcription factors; TOM, topological overlap matrix; GO, Gene Ontology; KEGG, Kyoto Encyclopedia of Genes and Genomes.
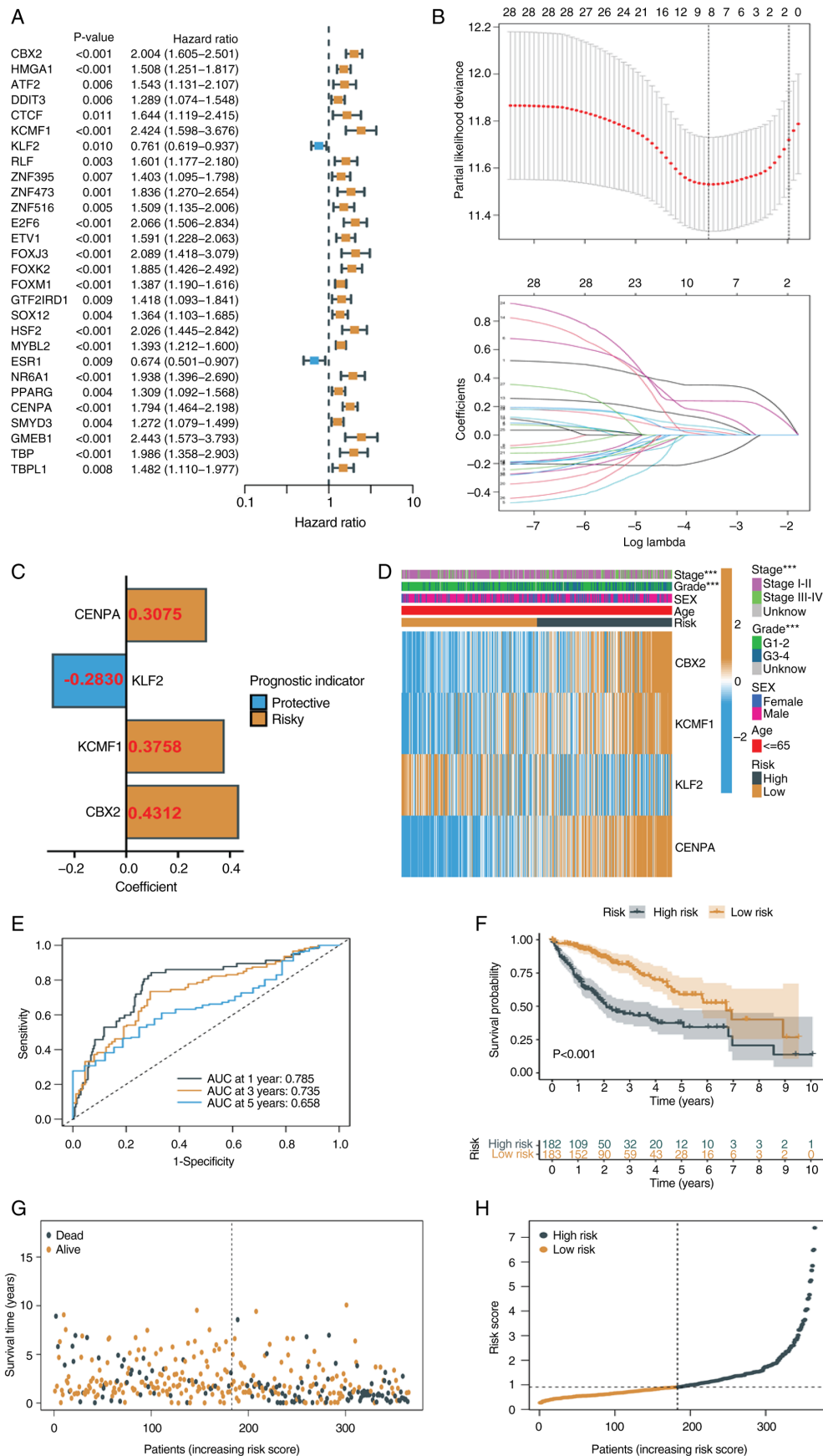
Figure 3. Construction of prognostic TRTs signature. (A) Univariate Cox regression analysis was used to identify TRTs significantly associated with prognosis. (B) LASSO regression analysis (ENTER method) to remove redundant TRTs for further screening. (C) The four TRTs involved in modeling and their coefficient. (D) Heat map of expression of four TRTs and their relationship between clinical features. (E) ROC curves for predicting patient survival at 1, 3 and 5 years. (F) Kaplan-Meier analysis of differences in survival among patients with different risk groups. (G) Scatter plot and (H) curve plot of different risk scores. TRTs, TACE refractoriness-related transcription factors; LASSO, least absolute shrinkage and selection operator; ROC, receiver operating characteristic; AUC, area under curve.
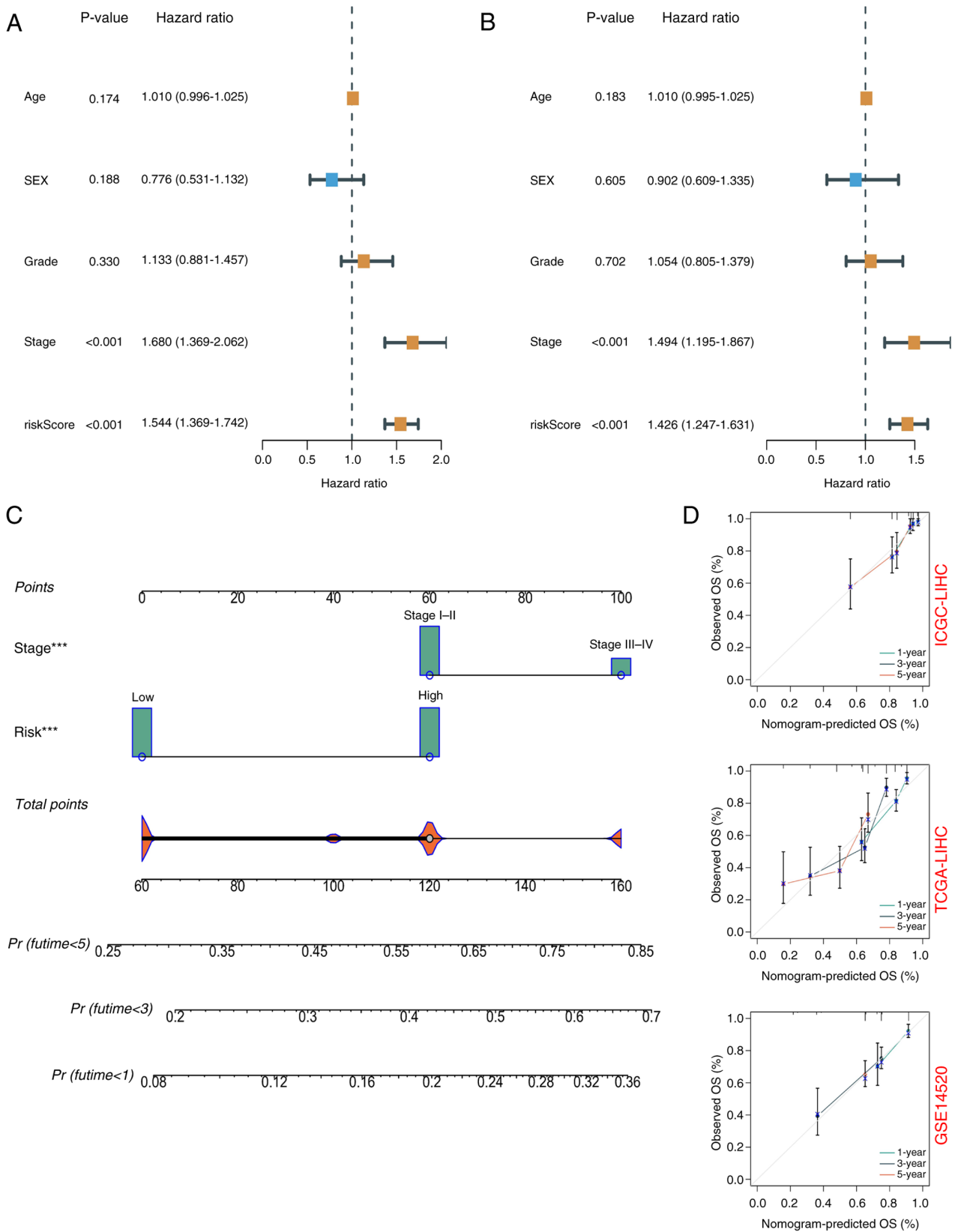
Figure 4. Assessment of the prognostic signature. (A) Univariate analysis and (B) multivariate analysis of risk score and clinical characters in TCGA cohort. (C) Nomograms and (D) calibration plots were used to quantify the contribution of individual factors to clinical outcomes and to verify the validity of the model. TCGA, The Cancer Genome Atlas. ***P<0.001.

same formula and cutoff as for TCGA-LIHC, with high- and low-risk groups, to confirm the external validity of the prognostic model. A total of 108 low-risk and 123 high-risk patients

from the ICGC-LIHC group were found. In the GSE14520 cohort, 107 high-risk and 114 low-risk patients were identified. In the ICGC-LIHC cohort, the risk score was an independent

prognostic indicator (Fig. 5A and B) and survival time decreased significantly with increasing risk score (Fig. 5C-E). ROC curve analysis also showed the excellent predictive power of the risk score (1-year AUC, 0.755; 3-year AUC, 0.799; 5-year AUC, 0.730; Fig. 5F). In the GSE14520 cohort, the risk score was also an independent prognostic factor and a good predictor of survival risk (Fig. 5G-L).

*Analysis of immune infiltration.* In addition to TACE therapy, patients with liver cancer can also receive immunotherapy to improve the therapeutic effect. Immune infiltrating cells are a key part of the TME, which is vital for tumor development, therapy response and patient prognosis. The present study assessed TME as a whole in TCGA-LIHC cohort using the ESTIMATE algorithm and found that tumor purity scores increased and immune scores decreased as the risk scores increased (Fig. 6A and B). Increasing evidence suggests that there is a strong correlation between enhanced stem-cell-related biomarker expression in tumor cells and drug resistance, cancer recurrence and tumor growth (41). Thus, the relationship between the risk scores and DNA stem cell score (DNAss) and RNA stem cell score (RNAss) were evaluated. The present study revealed a substantial positive correlation between the risk score and DNA and RNA concentrations. The gene mutation status of the groups with high and low risk scores was also compared. Considering the important effect of stemness index on immunotherapy, correlation analysis showed that DNAss and RNAss increased with risk score (Fig. 6C and D). The identified immune subtypes were analyzed. Thorsson *et al* (19) defined six immunoexpression signature subtypes based on the gene expression profile of all solid tumors in TCGA, including Wound Healing (Immune C1), IFN-γ Dominant (Immune C2), Inflammatory (Immune C3), Lymphocyte Depleted (Immune C4), Immunologically Quiet (Immune C5) and TGF-β Dominant (Immune C6). The present study found a higher proportion of the lymphocyte depleted subtype in high-risk patients and the highest expression of the risk scores in the Wound Healing subtype (Fig. 6E and F). To determine the number of immune cells present in various samples, a variety of algorithms were used, including TIMER, CIBERSORT, QUANTISEQ, MCP-counter, XCELL and EPIC. The abundance of killer immune cells, such as CD4$^+$ and CD8$^+$ T cells, increased as the risk score increased (Fig. 6G). At the same time, there were also differences in the distribution of immune cells among the different risk subtypes (Fig. 6H). To verify the survival prediction and treatment reflection predictive value of the risk score in the immunotherapy cohort, it was tested in different Imvigor-210 immunotherapy cohorts. The results showed that the risk score also had a prognostic value in different immunotherapy cohorts (Fig. 6I). In low-risk patients, there was an improved response to immunotherapy, with complete response/partial response accounting for 29% compared with 17% in high-risk patients (Fig. 6J).

*Expression and prognostic profile of four TRTs.* The present study compared the expression profiles of four TRTs in normal and tumor tissues obtained from TCGA and Genotype-Tissue Expression databases, including paired and unpaired samples. Expression of CENPA, KCMF1 and CBX2 in tumor tissues

was significantly higher than in normal tissues, while expression of KLF2 was not significantly different (Fig. 7A and B). Expression of the aforementioned four TRTs in different groups in the Human Protein Atlas (HPA) database were detected. Protein expression was more consistent with mRNA expression. Compared with normal tissue, protein staining in tumor tissue was stronger (Fig. 7C). Cox regression analysis was performed on expression of CENPA, KCMF1, CBX2, KLF2 and various prognostic outcomes in multiple HCC cohorts. KCMF1 was a risk factor in four cohorts (Fig. 7D); CBX2 was a risk factor in cohorts (Fig. 7E); CENPA was a risk factor in eight cohorts (Fig. 8A); and KLF2 was a protective factor in six cohorts (Fig. 8B). These results demonstrated that the prognostic indicators of different TRTs were consistent.

*Drug sensitivity analysis.* Due to the limitations of systemic chemotherapy, most patients with advanced HCC have the option of local therapy based on TACE, which delivers chemotherapeutic drugs to the region surrounding the tumor (42). According to the enrichment analysis discussed aforementioned, patients in the various risk groups may have variable medication sensitivity and metabolism. The present study measured IC$_{50}$ values of the drugs frequently used in the treatment of HCC, such as vincristine, sorafenib, mitomycin, etoposide, doxorubicin and cisplatin. The IC$_{50}$ value of platinum was significantly lower in the high-risk group than in the low-risk group (both P<0.05) (Fig. 8C-H). These results suggested that high-risk patients were more sensitive to commonly used chemotherapy and targeted drug therapy for HCC.

*Risk score at a single-cell level treated with ICIs.* Considering bulk-RNA-sequencing data, risk scores based on CENPA, KLF2, KCMF1 and CBX2 are good indicators of TME. Therefore, analyses were performed in the GSE125449 single-cell sequencing dataset, to assess changes in risk scores in various types of cell before and after ICI treatment. The GSE125449 single-cell sequencing dataset was annotated based on the TISCH database (Fig. 9A) and the risk scores in different cells were calculated. Expression of risk scores was higher in interstitial cells (Fig. 9B). After treatment with ICIs, the risk score increased in tumor cells but decreased in stromal cells (Fig. 9C). Cell-type-specific analyses was performed and showed that the risk scores in liver progenitors changed significantly after ICI treatment (Fig. 9D).

*Validation of TRTs in HCC cell lines.* SNU-387 and Huh7 cells were simultaneously cultured under hypoxia (1% O$_2$) and normoxia for 48 h to mimic TACE. The present study detected the IC$_{50}$ of lobaplatin, the first-line drug for TACE treatment, in these cell types. Compared with normal oxygen concentration, the IC$_{50}$ of SNU-387 lobaplatin cultured under hypoxia was significantly higher, while that of Huh7 was significantly lower (Fig. 10A). This indicates that SNU-387 is a TACE-resistant cell line and Huh7 is a TACE nonresistant cell line. We detected expression of the four TRTs in these two cell lines. CENPA, KCMF1 and CBX2, which are high-risk factors, were higher in the resistant cell line SNU-387 than in Huh7 cells. However, KLF2, the protective factor, showed no difference in expression between the two cell lines (Fig. 10B).
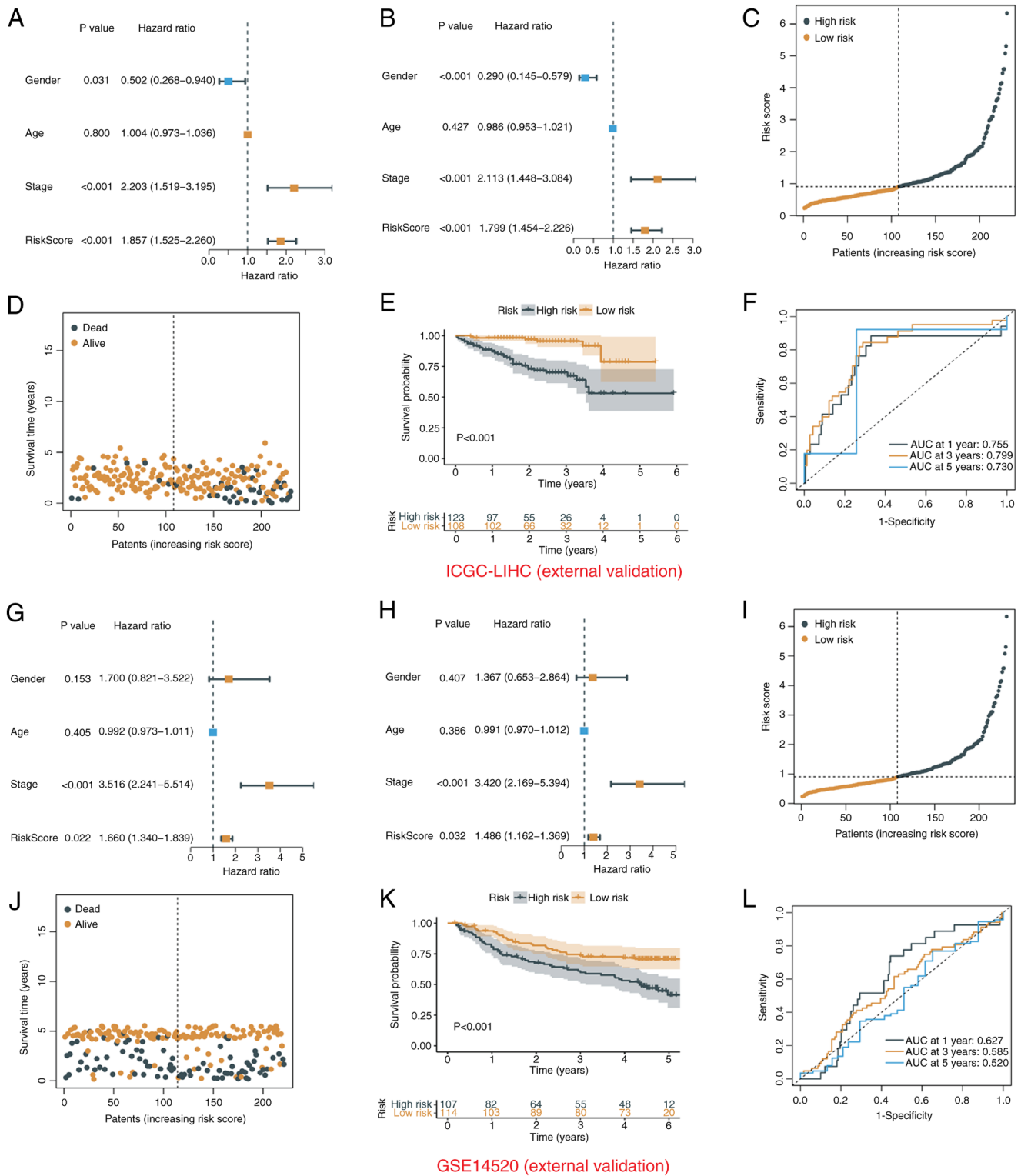
Figure 5. Validation of prognostic TRT signature in external datasets. (A) Univariate and (B) multivariate regression were used for validation of risk score in ICGC-LIHC cohort. (C) Curve plot and (D) scatter plot between different risk groups in the ICGC-LIHC cohort. (E) Kaplan-Meier survival curves of OS and (F) ROC curves of the TRT signature in the ICGC-LIHC cohort. (G) Univariate and (H) multivariate regression were used for validation of risk score in GSE14520 cohort. (I) Curve plot and (J) scatter plot between different risk groups in the GSE14520 cohort. (K) Kaplan-Meier survival curves of OS and (L) ROC curves of the TRT signature in the GSE14520 cohort. TRTs, TACE refractoriness-related transcription factors; OS, overall survival; ROC, receiver operating characteristic; AUC, area under curve.

## Discussion

Primary liver cancer, characterized by high incidence and mortality rates, is a malignant tumor that poses a serious threat

to the lives and health of patients (43). Despite continuous advances in treatment methods in recent years, the overall efficacy of liver cancer therapy remains suboptimal. The present study explored the mechanisms by which TFs influence liver
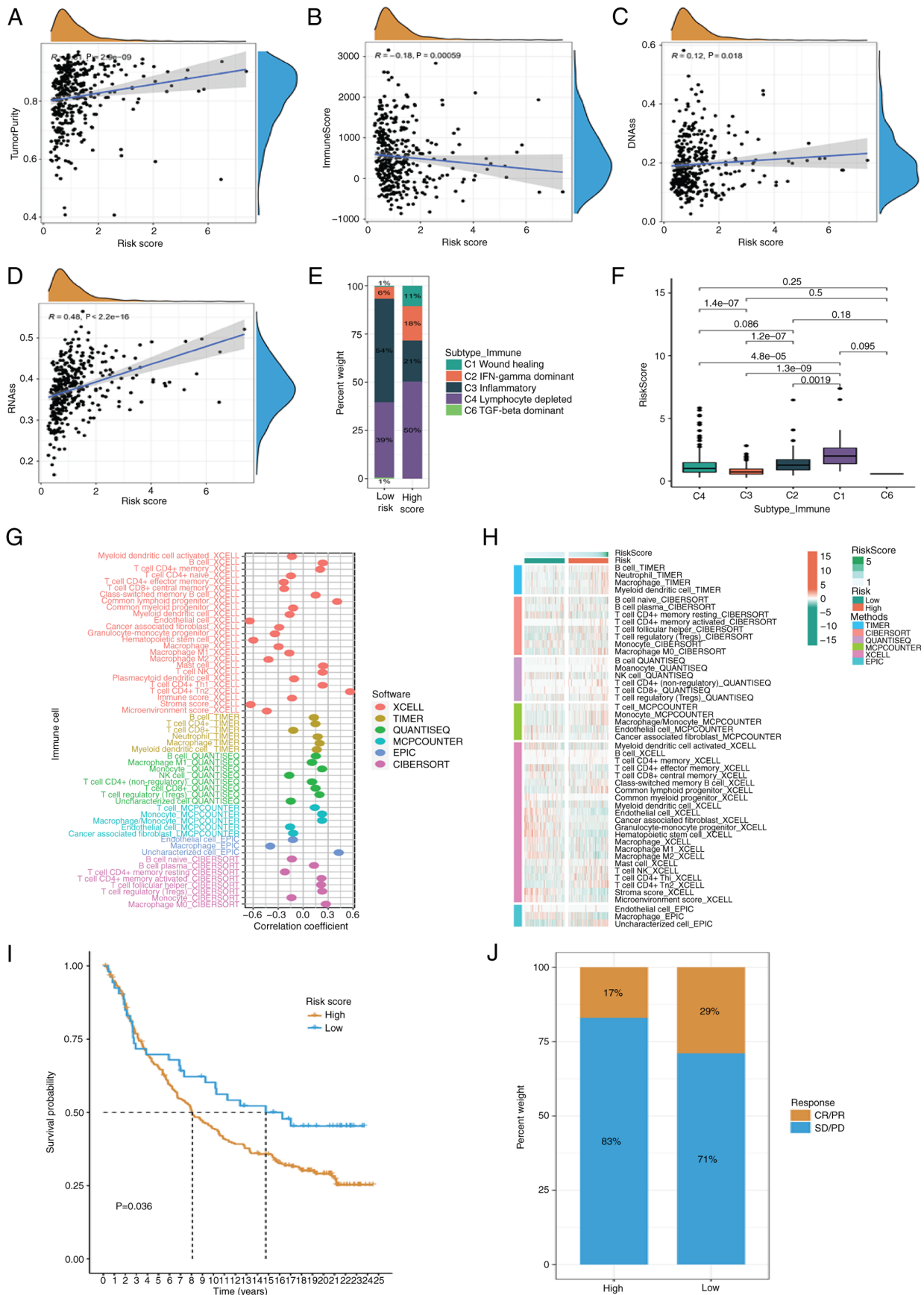
Figure 6. Analysis of immune infiltration. ESTIMATE algorithm was used to evaluate TME. (A) Tumor purity, (B) immune score, (C) correlation of DNAss and (D) RNAss with different risk score. (E and F) Percentage of identified immune subtypes in patients at different risk. (G) Different algorithms such as TIMER, CIBERSORT, QUANTISEQ, MCP-counter, XCELL and EPIC were used to estimate immune cell abundance in different samples. (H) Differences in the distribution of immune cells in different risk subtypes. (I) Imvigor-210 immunotherapy cohort was used to validate the prognostic value of risk scores. (J) Proportion of complete/PR and SD/PD in different risk groups. DNAss, DNA stem cell score; RNAss, RNA stem cell score; PR, Partial Response; SD, Stable Disease; PD, Progressive Disease
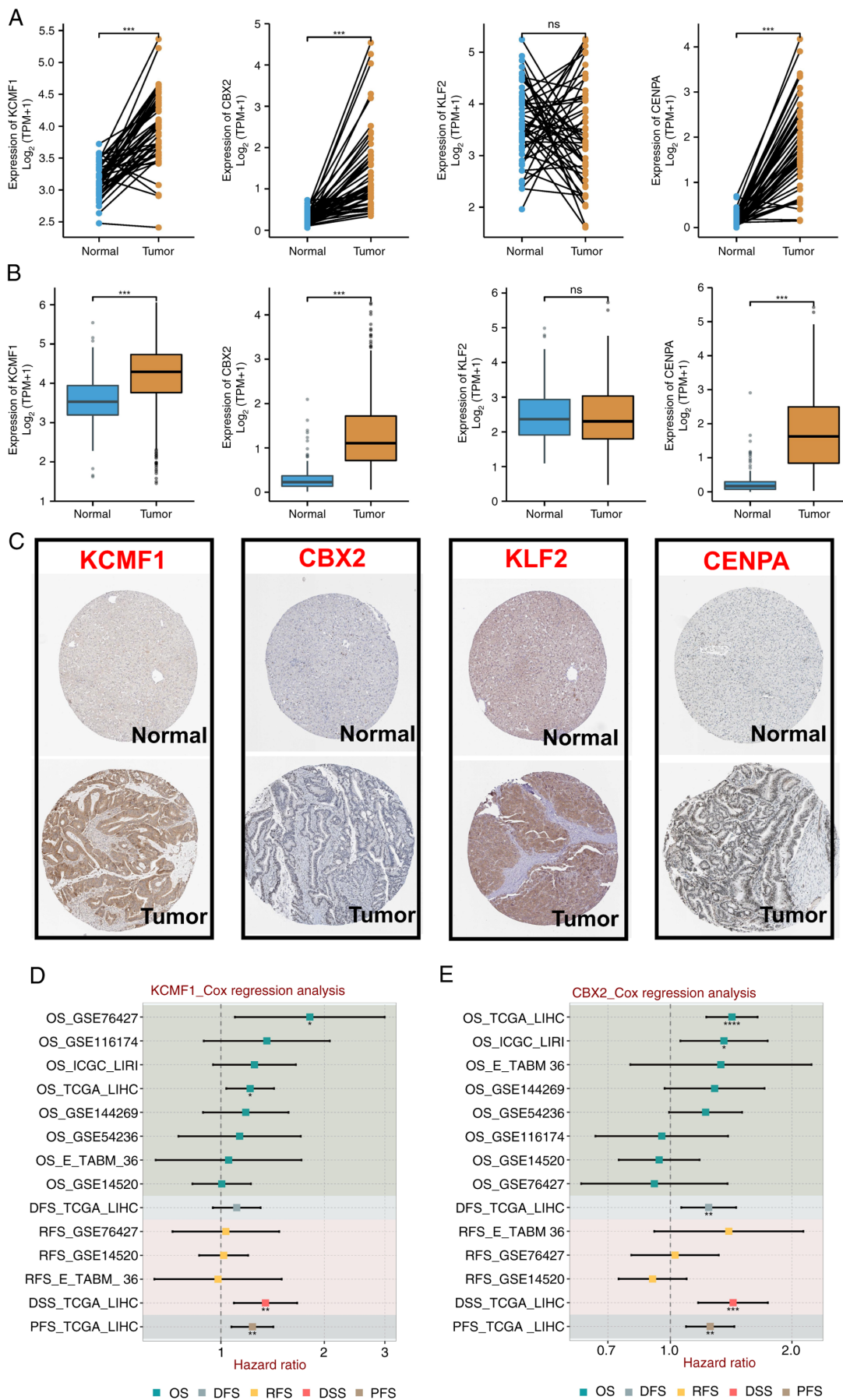
Figure 7. Expression and prognostic profile of four TRTs. (A and B) Expression of four signatures in normal and HCC tissues were compared by combining TCGA and GTEx databases. (C) Comparison of expression of four TRTs in different tissues using HPA database. Multiple HCC cohorts were used to validate (D) KCMF1 and (E) CBX2 expression and prognostic prediction. TRTs, TACE refractoriness-related transcription factors; HCC, hepatocellular carcinoma; TCGA, The Cancer Genome Atlas; GTEx, Genotype-Tissue Expression. *P<0.05, **P<0.01, ***P<0.001 and ****P<0.0001.
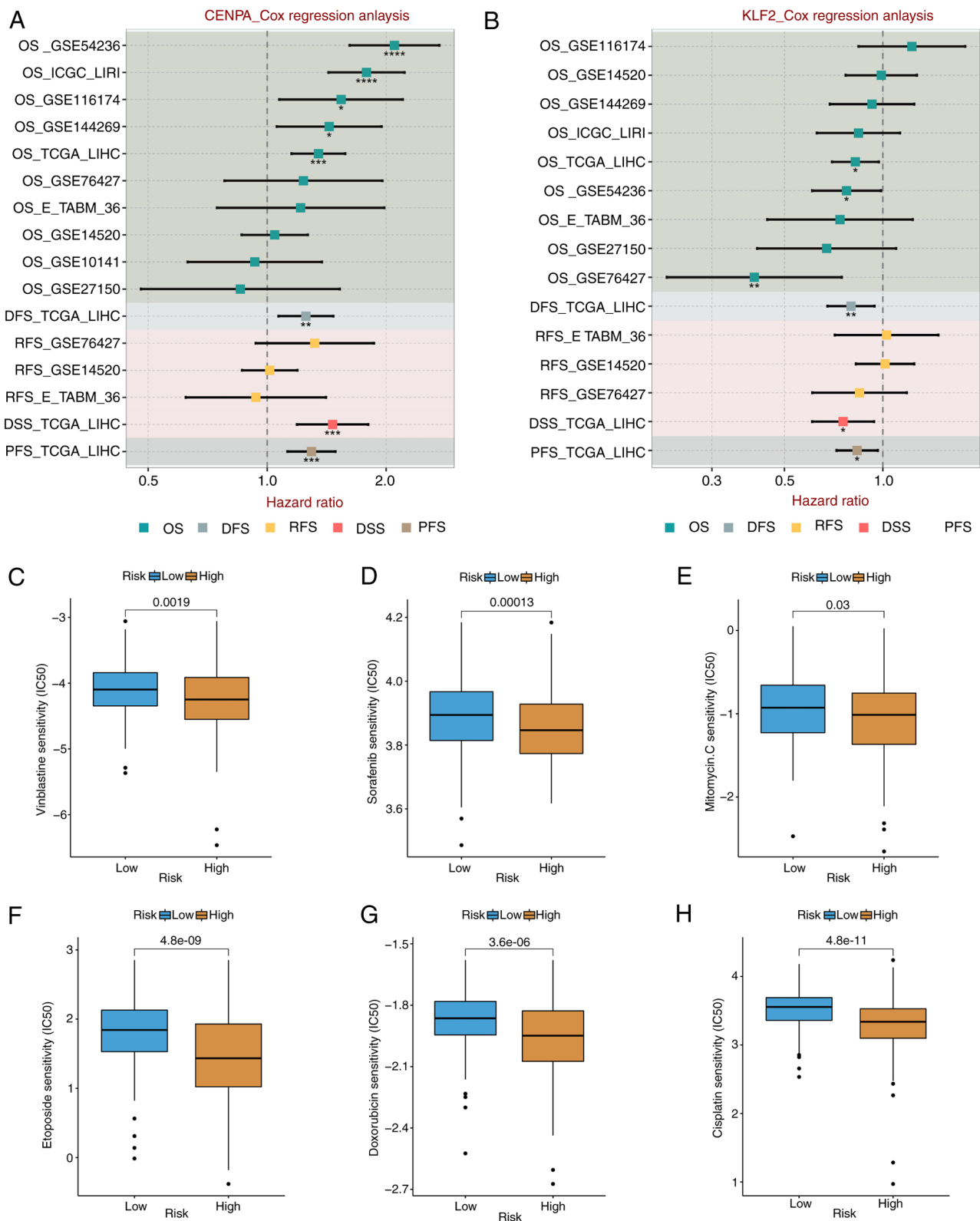
Figure 8. Different cohort validation and drug sensitivity analysis. Multiple HCC cohorts were used to validate (A) CENPA and (B) KLF2 expression and prognostic prediction. GDSC database was used to detect the $IC_{50}$ values of patients with different risk groups for commonly used clinical TACE drugs such as (C) vinblastine, (D) sorafenib, (E) mitomycin, (F) etoposide, (G) doxorubicin and (H) cisplatin. HCC, hepatocellular carcinoma; GDSC, Genomics of Cancer Drug Sensitivity; $IC_{50}$, half-maximal inhibitory concentration; TACE refractoriness-related transcription factors. $^*P<0.05$, $^{**}P<0.01$, $^{***}P<0.001$ and $^{****}P<0.0001$.

cancer, thereby providing new insights for improving therapeutic strategies.

The limited effectiveness of current treatments prompts a critical re-evaluation of existing therapeutic approaches and

highlights gaps in our understanding. While the pivotal role of TFs in tumor progression is well recognized, their specific mechanisms in TACE remain inadequately elucidated. This knowledge gap presents a crucial research opportunity to delve
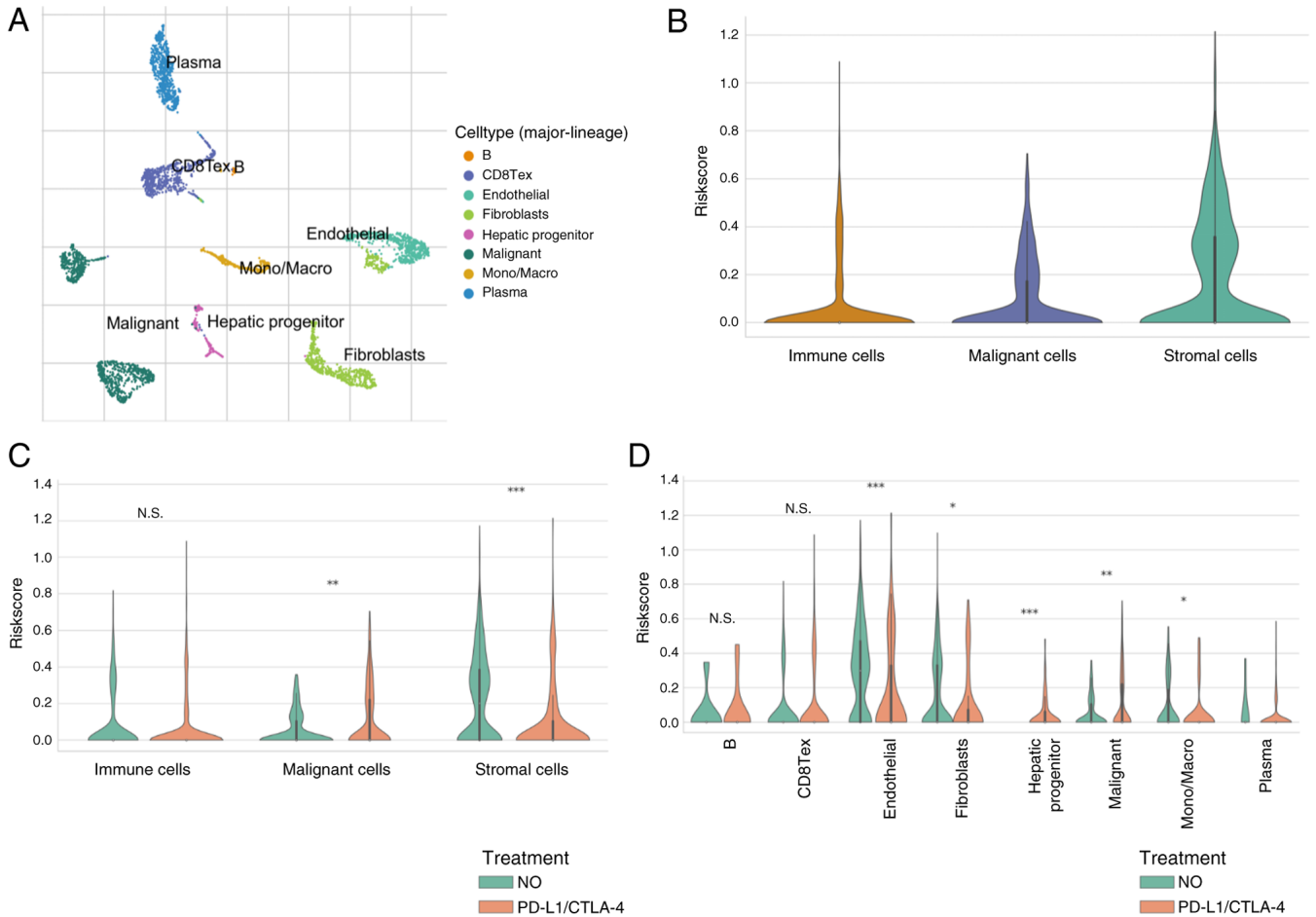
Figure 9. Risk score in single cells treated with ICIs. (A) Annotation of the GSE125449 single-cell sequencing dataset based on the TISCH database. (B) Correlation between risk score and TME status. (C) Correlation between risk score and TME status following ICI treatment. (D) Correlation between different types of cells and risk score following ICI treatment. ICIs, immune checkpoint inhibitors; TME, tumor microenvironment. $^*$P<0.05, $^{**}$P<0.01, $^{***}$P<0.001 and $^{****}$P<0.0001.
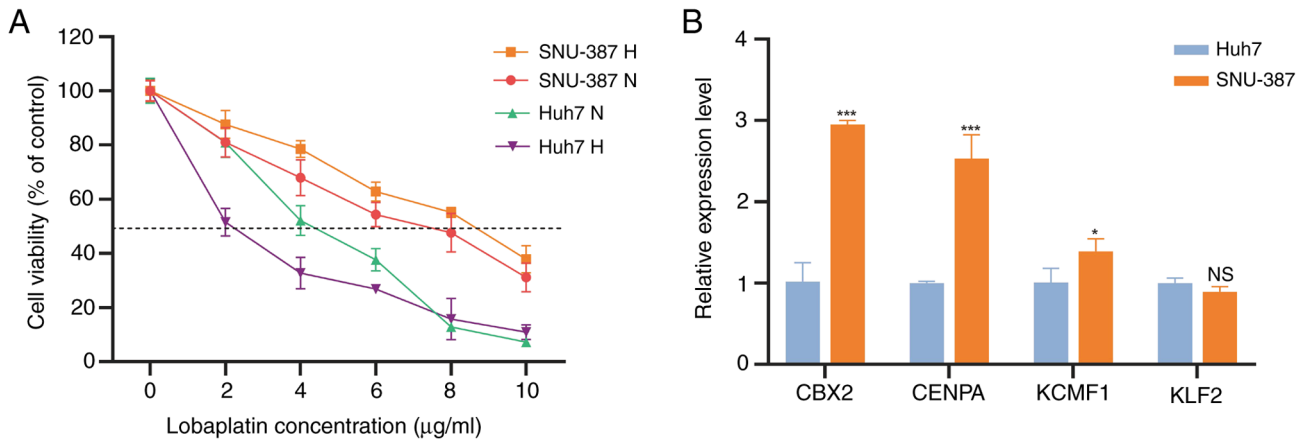


Figure 10. Validation of the TRTs in HCC cell lines. (A) IC$_{50}$ of SNU-387 and Huh7 for lobaplatin under normoxia and hypoxia (1% O$_2$). (B) Relative expression of four TRTs in Huh7 and SNU-387 cells. TRTs, TACE refractoriness-related transcription factors; HCC, hepatocellular carcinoma; IC$_{50}$, half-maximal inhibitory concentration. $^*$P<0.05; $^{***}$P<0.001.

into the function of TFs and to investigate their role in TACE resistance, ultimately aiming to optimize treatment regimens.

TFs play a crucial role in tumor progression by sustaining tumor stemness and regulating the TME, thereby driving cancer development (44). As our understanding of the functions of TFs deepens, it is expected that in the next 5 years, there will be more research focused on their application in TACE. Specifically, studies on how targeting TFs can overcome TACE resistance could lead to significant breakthroughs in liver cancer treatment (45).

Given the critical role of TFs and poor prognosis of patients following TACE, the present study developed a prognostic

model based on TFs to more accurately assess patient risk and guide personalized treatment. The model demonstrated potential value in evaluating the efficacy of TACE, particularly in predicting the prognosis of high-risk patients. However, the limitations of the model cannot be overlooked, primarily concerning the sources and quality of the data. Future research should focus on validating the model and exploring its applicability across different populations.

The present study systematically analyzed the role of transcription-related genes in TACE of HCC patients. It screened and constructed the predictive model including CENPA, KLF2, KCMF1 and CBX2 for risk assessment of liver cancer patients to determine the degree of benefit from TACE. Among these genes, CENPA, which encodes a protein that epigenetically determines the location of the centromere on each chromosome (46), was significantly upregulated in liver cancer tissues. It is considered important for metastatic ability and advanced disease status and may be a biomarker of poor prognosis and a high likelihood of recurrence (47). As a protective factor in this model, KLF2 (a host TF that regulates C-C chemokine receptor 5 expression in CD4$^+$ T cells) is involved in a variety of biochemical processes in humans, including lung development, embryonic erythropoiesis, epithelial integrity, T cell viability and adipogenesis (48). Although KLF2 has been shown to play a role in promoting tumor progression in a variety of tumors, there may be changes in a number of pathways due to the unique hypoxia and chemotherapeutic drug microenvironment of TACE (49), which needs to be further explored. There are few reports on the relationship between KCMF1 and tumors. As an evolutionarily highly conserved protein, increased expression of KCMF1 in the nucleus may be closely related to pancreatic cancer in mice and humans (50). CBX2 is associated with prognosis of liver cancer (51).

The present study intersected the genes in the TF module most associated with TACE response in GSE104580 with the differential genes in this dataset. As the GSE104580 dataset lacks survival data, the intersected gene set was placed in TCGA-LIHC cohort for LASSO-Cox analysis and four TRTs were identified to build a predictive model. Based on the predictive model, the patients were divided into high- and low-risk groups and the stability of the model verified. Immunotherapy provides a new option for liver cancer. The combination of TACE and immunotherapy has become a new strategy for advanced liver cancer. It has been shown that immunotherapy after TACE can prolong and maximize the immune response to liver cancer by preventing T-cell exhaustion (12). The combination of TACE and programmed death protein-1 in the treatment of advanced HCC can significantly prolong OS (11). Immune scores were significantly lower in high-risk patients. Comparing the identified immune subtypes, a higher proportion of the Lymphocyte Depleted subtype was found in high-risk patients. After analysis using various immune infiltration algorithms, it was found that the abundance of killer immune cells, such as CD4$^+$ and CD8$^+$ T cells, was increased in high-risk patients. KLF2 in the model negatively controlled the responsiveness of CD8$^+$ T cells to the C-X-C chemokine receptor 3 ligand CXCL10, which is consistent with the results of the present study (52). Sorafenib, doxorubicin and cisplatin are the first-line drugs for TACE and the IC$_{50}$ in the high-risk group was significantly lower than that in the low-risk group. This suggested that high-risk patients may be superior candidates for TACE and targeted drug therapy. Single-cell analysis can provide guidance for precise immunotherapy of tumors. Mesenchymal stem/stromal cells have high immunomodulatory activity, are easy to obtain and isolate and have a strong tropism for inflamed and damaged tissues (53). RNA was extracted from common liver cancer cell lines. RT-qPCR of genes in the four models revealed the highest expression of CENPA, CBX2 and CENPA in resistant cells, which was consistent with the hypothesis.

The present study focused on TFs closely related to TACE. The predictive model based on TFs was constructed to predict the prognosis of TACE patients. It was hypothesized that this model can provide new options for combined immunization and targeted therapy for TACE patients. However, the present study still had some limitations. First, the data were from public databases and lacked more data for verification. Second, the specific regulatory mechanism between TFs and TACE resistance remain to be elucidated, which requires further research.

The prognosis and TME status of liver cancer patients following TACE can be assessed using the predictive model based on the TF correlation created in the present study. This predictive model provides a reliable and simplified method to guide the clinical treatment of HCC patients.

## Availability of data and materials

The data generated in the present study are included in the figures and/or tables of this article.

## Authors' contributions

YS and JShi contributed to the conceptualization. XW and FJ performed the data analyses. JShen participated in data analysis and study design. JShi wrote the manuscript. JShen reviewed and edited the manuscript. YS and JShen confirm the authenticity of all the raw data. JZ interpreted data. All authors read and approved the final manuscript.

## Ethics approval and informed consent

Not applicable.

## Patient consent for publication

Not applicable.

## Competing interests

The authors declare that they have no competing interests.

## References

1. Bray F, Laversanne M, Sung H, Ferlay J, Siegel RL, Soerjomataram I and Jemal A: Global cancer statistics 2022: GLOBOCAN estimates of incidence and mortality worldwide for 36 cancers in 185 countries. CA Cancer J Clin 74: 229-263, 2024.

2. Di Bisceglie AM: Hepatitis B and hepatocellular carcinoma. Hepatology 49 (5 Suppl): S56-S60, 2009.

3. Deng ZJ, Li L, Teng YX, Zhang YQ, Zhang YX, Liu HT, Huang JL, Liu ZX, Ma L and Zhong JH: Treatments of hepatocellular carcinoma with portal vein tumor thrombus: Current status and controversy. J Clin Transl Hepatol 10: 147-158, 2022.

4. Frenette CT, Osorio RC, Stark J, Fok B, Boktour MR, Guy J, Rhee J and Osorio RW: Conventional TACE and drug-eluting bead TACE as locoregional therapy before orthotopic liver transplantation: Comparison of explant pathologic response. Transplantation 98: 781-787, 2014.

5. Miksad RA, Ogasawara S, Xia F, Fellous M and Piscaglia F: Liver function changes after transarterial chemoembolization in US hepatocellular carcinoma patients: The LiverT study. BMC Cancer 19: 795, 2019.

6. Sergio A, Cristofori C, Cardin R, Pivetta G, Ragazzi R, Baldan A, Girardi L, Cillo U, Burra P, Giacomin A and Farinati F: Transcatheter arterial chemoembolization (TACE) in hepatocellular carcinoma (HCC): The role of angiogenesis and invasiveness. Am J Gastroenterol 103: 914-921, 2008.

7. Kudo M, Matsui O, Izumi N, Kadoya M, Okusaka T, Miyayama S, Yamakado K, Tsuchiya K, Ueshima K, Hiraoka A, *et al*: Transarterial chemoembolization failure/refractoriness: JSH-LCSGJ criteria 2014 update. Oncology 87 (Suppl 1): S22-S31, 2014.

8. Sahin TK, Rizzo A, Aksoy S and Guven DC: Prognostic significance of the royal Marsden hospital (RMH) score in patients with cancer: A systematic review and Meta-analysis. Cancers (Basel) 16: 1835, 2024.

9. Rizzo A, Ricci AD and Brandi G: Trans-arterial chemoembolization plus systemic treatments for hepatocellular carcinoma: An update. J Pers Med 12: 1788, 2022.

10. Rizzo A, Dadduzio V, Ricci AD, Massari F, Di Federico A, Gadaleta-Caldarola G and Brandi G: Lenvatinib plus pembrolizumab: The next frontier for the treatment of hepatocellular carcinoma? Expert Opin Investig Drugs 31: 371-378, 2022.

11. Qin J, Huang Y, Zhou H and Yi S: Efficacy of sorafenib combined with immunotherapy following transarterial chemoembolization for advanced hepatocellular carcinoma: A Propensity Score Analysis. Front Oncol 12: 807102, 2022.

12. Zhang JX, Chen P, Liu S, Zu QQ, Shi HB and Zhou CG: Safety and efficacy of transarterial chemoembolization and immune checkpoint inhibition with camrelizumab for treatment of unresectable hepatocellular carcinoma. J Hepatocell Carcinoma 9: 265-272, 2022.

13. Rizzo A, Ricci AD and Brandi G: Systemic adjuvant treatment in hepatocellular carcinoma: Tempted to do something rather than nothing. Future Oncol 16: 2587-2589, 2020.

14. Latchman DS: Transcription factors: An overview. Int J Biochem Cell Biol 29: 1305-1312, 1997.

15. Bushweller JH: Targeting transcription factors in cancer-from undruggable to reality. Nat Rev Cancer 19: 611-624, 2019.

16. He Q, Li W, Ren J, Huang Y, Huang Y, Hu Q, Chen J and Chen W: ZEB2 inhibits HBV transcription and replication by targeting its core promoter. Oncotarget 7: 16003-16011, 2016.

17. Takada H and Kurisaki A: Emerging roles of nucleolar and ribosomal proteins in cancer, development, and aging. Cell Mol Life Sci 72: 4015-4025, 2015.

18. Zhang G and Zhang G: Upregulation of FoxP4 in HCC promotes migration and invasion through regulation of EMT. Oncol Lett 17: 3944-3951, 2019.

19. replot (Version sva v3.46.0) [Computer software]. 2023. Retrieved from https://github.com/jtleek/sva-devel.

20. Lambert SA, Jolma A, Campitelli LF, Das PK, Yin Y, Albu M, Chen X, Taipale J, Hughes TR and Weirauch MT: The human transcription factors. Cell 172: 650-665, 2018.

21. Hume MA, Barrera LA, Gisselbrecht SS and Bulyk ML: UniPROBE, update 2015: New tools and content for the online database of protein-binding microarray data on protein-DNA interactions. Nucleic Acids Res 43 (Database Issue): D117-D122, 2015.

22. Wingender E, Schoeps T, Haubrock M, Krull M and Dönitz J: TFClass: Expanding the classification of human transcription factors to their mammalian orthologs. Nucleic Acids Res 46: D343-D347, 2018.

23. replot (Version 4.0.5) [Computer software]. 2023. Retrieved from http://www.R-project.org/.

24. replot (Version limma v3.52.0) [Computer software]. 2023. Retrieved from https://bioconductor.org/packages/release/bioc/html/limma.html.

25. replot (Version pheatmap v1.0.12) [Computer software]. 2019. Retrieved from https://cran.r-project.org/web/packages/pheatmap/index.html.

26. replot (Version clusterProfiler v4.4.0) [Computer software]. 2023. Retrieved from https://bioconductor.org/packages/release/bioc/html/clusterProfiler.html.

27. replot (Version WGCNA v1.68) [Computer software]. 2021. Retrieved from https://cran.r-project.org/web/packages/WGCNA/index.html.

28. replot (Version v1.0.0) [Computer software]. 2023. Retrieved from https://cran.r-project.org/web/packages/replot/index.html.

29. replot (Version TIMER v2.0) [Computer software]. 2020. Retrieved from http://timer.cistrome.org/.

30. replot (Version CIBERSORT v1.06) [Computer software]. 2015. Retrieved from https://cibersort.stanford.edu/

31. replot (Version quanTIseq v1.0) [Computer software]. 2019. Retrieved from https://icbi.i-med.ac.at/software/quantiseq/doc/.

32. replot (Version MCP-counter v1.2.0) [Computer software]. 2021. Retrieved from https://github.com/ebecht/MCPcounter.

33. replot (Version xCell v1.1.0) [Computer software]. 2017. Retrieved from https://xcell.ucsf.edu/.

34. replot (Version EPIC v1.1) [Computer software]. 2020. Retrieved from https://gfellerlab.shinyapps.io/EPIC_1-1/.

35. replot (Version ESTIMATE v1.0.13) [Computer software]. 2013. Retrieved from https://bioinformatics.mdanderson.org/estimate/.

36. Yoshihara K, Shahmoradgoli M, Martinez E, Vegesna R, Kim H, Torres-Garcia W, Treviño V, Shen H, Laird PW, Levine DA, *et al*: Inferring tumour purity and stromal and immune cell admixture from expression data. Nat Commun 4: 2612, 2013.

37. Thorsson V, Gibbs DL, Brown SD, Wolf D, Bortone DS, Ou Yang TH, Porta-Pardo E, Gao GF, Plaisier CL, Eddy JA, *et al*: The immune landscape of cancer. Immunity 48: 812-30.e14, 2018.

38. Geeleher P, Cox NJ and Huang RS: Clinical drug response can be predicted using baseline gene expression levels and in vitro drug sensitivity in cell lines. Genome Biol 15: R47, 2014.

39. replot (Version pRRophetic v1.0.2) [Computer software]. 2024. Retrieved from https://github.com/paulgeeleher/pRRophetic2.

40. Livak KJ and Schmittgen TD: Analysis of relative gene expression data using real-time quantitative PCR and the 2(-Delta Delta C(T)) method. Methods 25: 402-408, 2001.

41. Luo Q and Vogeli TA: A Methylation-Based reclassification of bladder cancer based on immune cell genes. Cancers (Basel) 12: 3054, 2020.

42. Shin SW: The current practice of transarterial chemoembolization for the treatment of hepatocellular carcinoma. Korean J Radiol 10: 425-434, 2009.

43. Ananthakrishnan A, Gogineni V and Saeian K: Epidemiology of primary and secondary liver cancers. Semin Intervent Radiol 23: 47-63, 2006.

44. Islam Z, Ali AM, Naik A, Eldaw M, Decock J and Kolatkar PR: Transcription Factors: The Fulcrum Between Cell Development and Carcinogenesis. Front Oncol 11: 681377, 2021.

45. Caamano J and Hunter CA: NF-kappaB family of transcription factors: Central regulators of innate and adaptive immune functions. Clin Microbiol Rev 15: 414-429, 2002.

46. Fachinetti D, Folco HD, Nechemia-Arbely Y, Valente LP, Nguyen K, Wong AJ, Zhu Q, Holland AJ, Desai A, Jansen LE and Cleveland DW: A two-step mechanism for epigenetic specification of centromere identity and function. Nat Cell Biol 15: 1056-1066, 2013.

47. Mahlke MA and Nechemia-Arbely Y: Guarding the Genome: CENP-A-Chromatin in health and cancer. Genes (Basel) 11: 810, 2020.

48. Pearson R, Fleetwood J, Eaton S, Crossley M and Bao S: Kruppel-like transcription factors: A functional family. Int J Biochem Cell Biol 40: 1996-2001, 2008.

49. Suzuki H, Ohshima N, Tatei K, Taniguchi T, Sato S and Izumi T: The role of autonomously secreted $PGE_2$ and its autocrine/paracrine effect on bone matrix mineralization at the different stages of differentiating MC3T3-E1 cells. Biochem Biophys Res Commun 524: 929-935, 2020.

50. Beilke S, Oswald F, Genze F, Wirth T, Adler G and Wagner M: The zinc-finger protein KCMF1 is overexpressed during pancreatic cancer development and downregulation of KCMF1 inhibits pancreatic cancer development in mice. Oncogene 29: 4058-4067, 2010.

51. Wang X, Lu Y, Li C, Larbi A, Feng L, Shen Q, Chong MS, Lim WS and Feng L: Associations of lifestyle activities and a heathy diet with frailty in old age: A Community-based study in Singapore. Aging (Albany NY) 12: 288-308, 2020.
52. Preston GC, Feijoo-Carnero C, Schurch N, Cowling VH and Cantrell DA: The impact of KLF2 modulation on the transcriptional program and function of CD8 T cells. PLoS One 8: e77537, 2013.
53. Zhuang WZ, Lin YH, Su LJ, Wu MS, Jeng HY, Chang HC, Huang YH and Ling TY: Mesenchymal stem/stromal Cell-based therapy: Mechanism, systemic safety and biodistribution for precision clinical applications. J Biomed Sci 28: 28, 2021.